J Solid State Electrochem (2012) 16:1263–1270
DOI 10.1007/s10008-011-1521-6

ORIGINAL PAPER

Significantly enhanced rate capability in supercapacitors using carbide-derived carbons electrode with superior microstructure

Gangwei Sun · Wenhua Song · Xiaojun Liu · Wenming Qiao · Donghui Long · Licheng Ling

Received: 18 April 2011 / Revised: 30 July 2011 / Accepted: 2 August 2011 / Published online: 17 August 2011

Abstract Mesoporous carbide-derived carbons (CDC) with hierarchical pore structure were fabricated by chlorine etching of mesoporous titanium carbides. Their capacitive behaviors for electrochemical capacitor were investigated in comparison to those of purely microporous CDC. The as-prepared mesoporous CDC exhibited not only uniform micropores formed by leaching out titanium atoms but a 3-D mesoporous network inherited from their parent carbides. These mesoporous CDC could deliver a high specific capacitance of 120 Fg^{-1} in 1 M tetraethylammonium tetrafluoroborate dissolved in propylene carbonate. Moreover, they owned excellent frequency response and superior rate capability with capacitance retention ratio of 91% at current density of 10 Ag^{-1}. A high energy density of 16.3 Wh kg^{-1} was obtained even though power density was raised up to 4,300 Wkg^{-1}. The distinctive capacitive performance of mesoporous CDC would be attributed to their superior microstructure, in which the uniform micropores contributed to high charge storage while the 3-D mesoporous network and nanometer-scaled dimension of particles facilitated ions transfer as well as shortened electrolyte diffusion distance.

Keywords Electrochemical capacitor · Carbide-derived carbon · Impedance · Rate capability · Kinetic process

Introduction

Electrochemical capacitors (EC) are extensively studied due to their promising properties in terms of energy storage and power supply, which could fill the gap between the secondary batteries and the conventional dielectric capacitors [1–3]. Although EC offer lower energy density than Li-ion batteries, they possess many attractive characteristics, not afforded by Li-ion batteries. For EC, a million charging–discharging cycles are typically degradation-free. This is many times more than for any known battery. Subminute charge and discharge without sacrificing their energy storage would allow broader implementation of EC in military and aerospace applications [4, 5]. The core technology of EC is the fabrication of high-performance electrode materials. Great efforts have been devoted to develop advanced nanostructured carbon electrode materials [5–9] and to understand the charge storage mechanisms [10–17].

Recently, an impressive synthesis method for advanced carbon has been developed through use of inorganic precursor carbides [18–23]. The resulting carbons were known as carbide-derived carbons (CDC). CDC were obtained by extraction of metals from carbides in halogens at elevated temperature, permitting atomic-level porosity control with a narrow unimodal pore-size distribution [18, 19]. Capacitance results demonstrated that ions could be partially or completely stripped of solvent sheath to occupy the subnanometer pores, leading to the anomalous capacitance increase in CDC with extremely small pores [15, 17]. These discoveries indicated electrode materials with uniform micropores were beneficial for their applications where energy density was at a premium, whereas small pores in CDC had an adverse effect on ion transport in inner pores. What is more, a long ion traveling distance related to the particle diameter would deteriorate high-rate charging–discharging properties of EC [24]. Therefore, optimizing CDC structure with high ion-accessible surface area, nanometer-scaled diffusion distance, and excellent electron conduction network is urgently recommended for the pulse power applications.

G. Sun · W. Song · X. Liu · W. Qiao · D. Long (✉) · L. Ling
State Key Laboratory of Chemical Engineering, East China University of Science and Technology,
Shanghai 200237, China
e-mail: longdh@mail.ecust.edu.cn

A study of CDC derived from SiC powders with 20 nm to 20 μm demonstrated the small particles facilitated the migration of ions inside the porous electrode, leading to the improvement in capacitance retention and a decrease of the time constant by up to ~33% [25]. However, the potential for enhanced performance in porous carbon was rather moderate, presumably due to the agglomerations of nanoparticles, resulting in a more difficult pathway for ion migration. Korenblit et al. introduced the ordered mesoporous channels in the SiC-derived carbons, which served as ion highways and allowed for very fast ion transport into CDC particles [26]. Chmiola et al. reported the monolithic CDC films for micro-EC, leading to a distinguished volumetric capacitance [27]. In our previous work, we have demonstrated a novel mesoporous CDC (M-CDC) which was prepared through sol–gel method followed by the carbothermal reaction and chlorine etching. We found that the homogeneous dispersion of carbon sources in titanium precursor matrix was essentially important during the sol–gel process, which influenced the carbothermal reduction and consequently the performance of resultant mesopores carbide. However, the hydrolysis rate of titanium (IV) isopropoxide in hydrogen peroxide system was too fast to ensure the uniform phase of sucrose and titanium precursor sol. In this paper, acetic acid and titanium *n*-butoxide was acted as dispersant and titanium sources, respectively, instead of hydrogen peroxide and titanium (IV) isopropoxide. The acetic acid could slow down the hydrolysis process of titanium *n*-butoxide and restrain the formation of TiO_2. The architectures of mesoporous CDC could be tuned flexibly by varying the mole ratio of titanium *n*-butoxide to sucrose based on the easy rate-controlled sol–gel step. Electrochemical results suggested that M-CDC had a great potential in electrode materials for EC which were able to supply both high energy density and power density.

Experimental

Materials preparation

Mesoporous TiC were synthesized via carbothermal reduction of organic–inorganic gels as reported in the previous work [28]. In a typical synthesis, sucrose of 2.26 g was dissolved in acetic acid of 10 ml under heating at 80 °C. Then titanium *n*-butoxide of 6.81 g was weighed to the solution at room temperature; successive stirring led to a deep red solution and then to gels. Xerogels would be obtained after drying first at 60 °C and later at 110 °C. The resultant xerogels were carbothermally reduced at 1,500 °C for 3 h under the protection of argon to achieve mesoporous TiC. The structure of mesoporous TiC can be tuned by varying the mole ratio of titanium *n*-butoxide to sucrose (*R*). In this work, three mesoporous TiC with *R* of 1.5, 2, and 3 were prepared, and the obtained samples were denoted as M-TiC-R.

As-synthesized M-TiC were treated under chlorine atmosphere at 900 °C for etching Ti atoms from carbide matrix. After the chlorination, samples were annealed in H_2 for 2 h at 600 °C to passivate the highly reactive dangling bonds and remove the residual chloride trapped in nanopores. Exact details of the chlorination technique have been reported previously [29]. The as-prepared mesoporous CDC samples were labeled as M-CDC-R. For comparison purposes, commercial titanium carbide powders (C-TiC) with particle size of ca. 8 μm and specific surface area of 1.5 $m^2\ g^{-1}$ from Sigma-Aldrich Company were also used as starting materials to produce conventional microporous CDC (C-CDC).

Characterization of samples

The morphologies of samples were observed under scanning electron microscopy (SEM; JEOL JSM-6700F) and transmission electron microscopy (TEM; JEOL 2100F). N_2 adsorption–desorption isotherms were carried out using a Micromeritics ASAP2020 analyzer at 77 K. Before the measurements, samples were degassed in vacuum at 473 K for at least 6 h. Brunauer–Emmett–Teller (BET) method was utilized to calculate the specific surface areas. The total pore volume was estimated from the adsorbed amount at a relative pressure of P/P_0=0.985. The pore-size distribution and micropore surface areas were determined using non-local density functional theory (DFT) model.

Electrochemical measurements

The carbon powders were processed into capacitor electrodes by mixing them of 95 wt.% with polyterafluoroethylene (60 wt.% water suspension) of 5 wt%, homogenized in a mortar and pestle, then rolled into a thin film of uniform thickness, and finally punched into pellets. Electrode pellets were left to dry in the vacuum oven at 80 °C for at least 8 h until the EC device with organic electrolyte was constructed. The EC was assembled in Teflon Swagelok® type two-electrode configuration in a glove box (Mikrouna); 1 M tetraethylammonium tetrafluoroborate salt (Et_4NBF_4) solution in propylene carbonate was employed as electrolyte. Galvanostatic charge–discharge tests were conducted to calculate the specific capacitance of samples using an Arbin SCTS supercapacitor testing system (Arbin Instrument, TN, USA). Capacitors were run 100 cycles for each current density with value from 0.1 to 10 $A\,g^{-1}$. Cyclic voltammetry (CV) and electrochemical impedance spectroscopy (EIS) were recorded with a PCI4/300 potentiostat (Gamry,

Warminster, PA, USA). CV was performed in the voltage range 0.0–2.5 V at voltage sweep rate of 20 and 100 mV s^{-1} and EIS with the frequency range from 1 mHz to 100 kHz, AC amplitude, 5 mV.

Results and discussion

Structural characteristics

The key for successful preparation of mesoporous CDC is ascribed to using mesoporous TiC as precursors, which have 3-D gel network and can succeed to the resultant CDC. Figure 1a shows the typical morphology of M-TiC-3, indicating it consists of interconnected rounded particles with size of 20–100 nm. The TEM observations (Fig. 1b) further reveal that TiC particles constitute a 3-D open network. And each particle commonly consists of three to four primary titanium carbide crystals with a quasi-regular shape. The self-supported characteristics of gel network could prevent the further aggregation of TiC nanoparticles. The amorphous carbon, which should be originated from pyrolysis of unconsumed sucrose, can also be observed in the network of TiC. These carbons consist of highly ramified and fibrous amorphous frameworks with a disordered mesoporous structure, as shown in Fig. 1c. The transformation of titanium carbide to carbon is known to be conformal at both the micrometer and the nanometer scales. The conserved shape is confirmed by the SEM and TEM images of mesoporous CDC (shown in Fig. 1d, e). The high-resolution TEM observation shows that TiC-derived carbon particles with a clear boundary are dispersed in the amorphous carbon matrix. The highly disordered microstructure of the TiC-derived carbon (Fig. 1f) is very similar to that observed in the prior studies of TiC-derived carbon [22].

N_2 adsorption–desorption isotherms of M-TiC are shown in Fig. 2. The resultant pores properties are compiled in Table 1. All isotherms are of type IV and exhibit a clear hysteresis loop, suggesting the presence of mesopores. The BET-specific surface areas (S_{BET}) decrease gradually with R increasing, whereas the average pore sizes increase from 3.6 to 14.4 nm. After the chlorination, N_2 adsorption–desorption isotherms of M-CDC exhibit a combined characteristic of type I/IV (Fig. 3a), in contrast to the type I isotherm for purely microporous C-CDC. M-CDC samples inherit the mesopores from their parent carbides in addition to developing micropores as the extraction of titanium atoms from the matrix. As depicted in Fig. 3b, all M-CDC samples have the similar distribution in micropores region (<2 nm), due to the same chlorination condition. The pore-size distribution curves become wider and shift toward larger pore size in the mesopores range with R increasing.

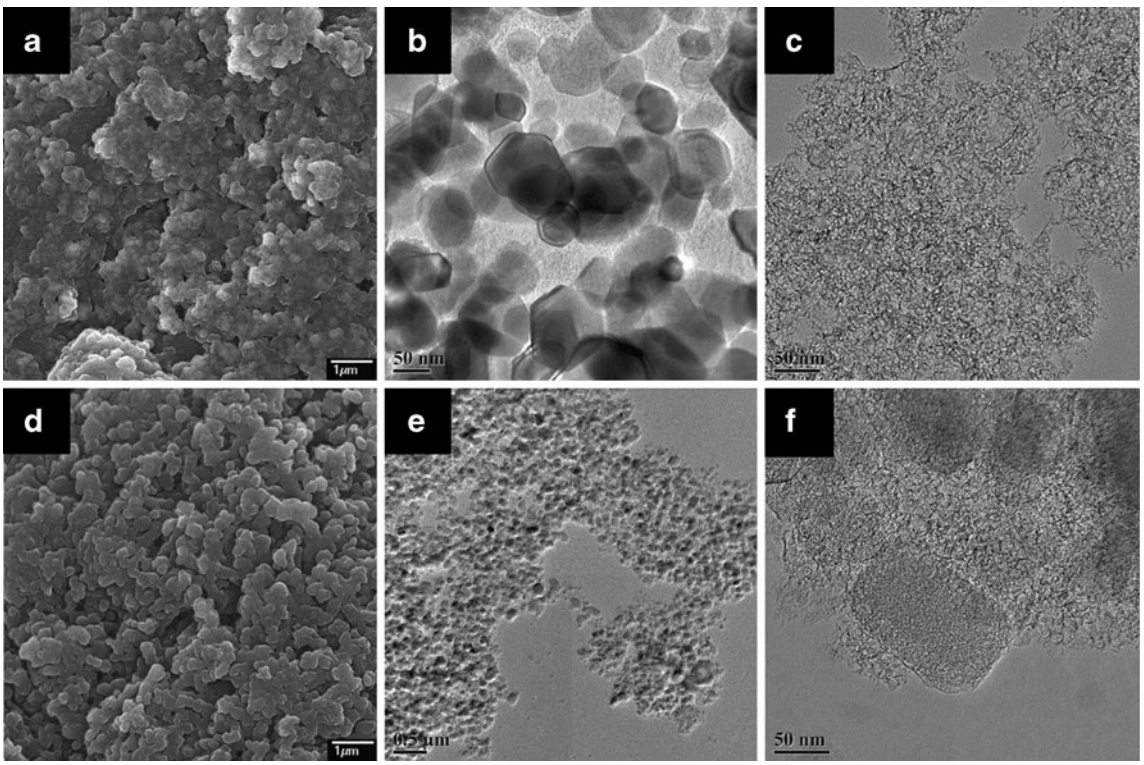

Fig. 1 Electron microscopy of samples: **a** SEM image of M-TiC, **b** TEM images of M-TiC, **c** TEM image of residual free carbon, **d** SEM image of M-CDC, **e**, **f** TEM images of M-CDC

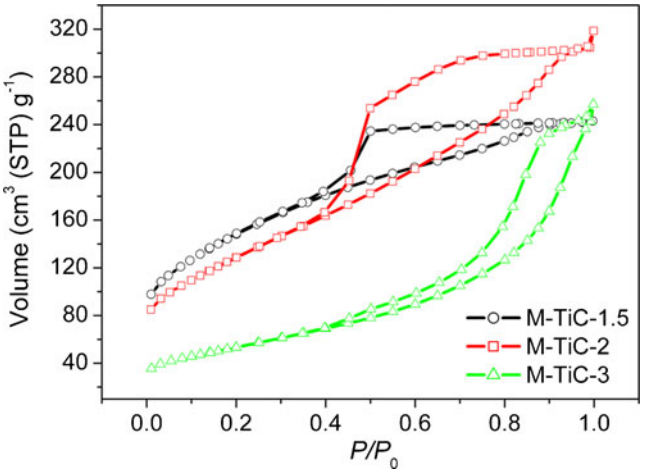

Fig. 2 N_2 adsorption–desorption isotherms of as-prepared mesoporous TiC samples

On the contrary, there are almost no distributions in the mesopores and macropores region for C-CDC. Table 1 summarizes the porosity parameters of CDC samples. M-CDC samples have slightly higher S_{BET} than that of C-CDC, whereas, their micropores specific surface areas (S_{micro}) are significantly lower than that of the latter.

Electrochemical properties

Galvanostatic charge/discharge between 0.0 and 2.5 V has been employed to estimate the electrochemical performance of samples, as shown in Fig. 4. All charge/discharge curves display the regularly triangular shape, which is indicative of the good columbic efficiency and ideal capacitor behavior. The gravimetric capacitance of sample is calculated according to $C = 2 \times I \times \Delta t/(\Delta V \times m)$, where C is gravimetric capacitance (farads per gram), I is the discharge current density (amperes), Δt is the discharge time (seconds) from 2.5 to 0 V, ΔV is the working voltage (volts), and m is the mass of single electrode (grams). The factor of 2 in this equation comes from the fact that the overall capacitance measured from the two-electrode system is the sum of two equivalent single electrode capacitors in series. Among all samples, C-CDC with the highest S_{micro} gives the largest gravimetric capacitance of 121.4 F g^{-1} at current density of 0.1 A g^{-1}. In comparison, the smaller gravimetric capacitance of 104.5, 109.7, and 112.5 F g^{-1} is obtained for M-CDC-1.5, M-CDC-2, and M-CDC-3, respectively, due to their relatively small proportion of micropores. The results prove that the gravimetric capacitances have a strongly dependent on S_{DFT}.

To evaluate the rate capability, the variation of gravimetric capacitance versus the charge/discharge current density is plotted in Fig. 5. Capacitances are calculated from the 100th cycle for each specific current density case. The gravimetric capacitance decreases with the current density increasing for all CDC samples. This indicates that there is always less electrochemically active surface area of pores being utilized at higher rate occasions. However, M-CDC samples provide superior capacitance retention at high discharge rates as compared to C-CDC material. Amazingly, with an increase of the current density from 0.1 to 10 A g^{-1}, a very small decrease in capacitance of only ~9% is observed for M-CDC-2. In contrast, C-CDC with pure micropores produced from dense TiC particles shows much obvious capacitance fading and a low capacitance retention ratio of ~70% at similarly high current density. These results highlight the suitability of M-CDC materials for high-rate application. Generally, the rate capability of capacitor is strongly determined by the penetration process

Table 1 Porosity parameters of TiC and CDC samples

Samples	S_{BET}[a] (m^2 g^{-1})	S_{DFT}[b] (m^2 g^{-1})	$S_{(<2\ nm)}$[c] (m^2 g^{-1})	$S_{(>2\ nm)}$[d] (m^2 g^{-1})	V_t[e] (cm^3 g^{-1})	D_{BJH}[f] (nm)
M-TiC-1.5	590	/	/	/	0.44	3.6
M-TiC-2	454	/	/	/	0.47	3.9
M-TiC-3	171	/	/	/	0.37	14.4
C-TiC	1.5	/	/	/	/	/
M-CDC-1.5	1,479	1,224	937	287	1.06	3.2
M-CDC-2	1,592	1,301	822	479	1.48	3.8
M-CDC-3	1,674	1,316	930	386	2.03	14.2
C-CDC	1,436	1,595	1,557	38	0.80	/

[a] Calculated using BET model

[b] Calculated using DFT model

[c] Calculated surface area of pore size smaller than 2 nm using DFT model

[d] Calculated surface area of pore size larger than 2 nm using DFT model

[e] Total pore volume calculated at the P/P_0=0.985

[f] BJH desorption pore size

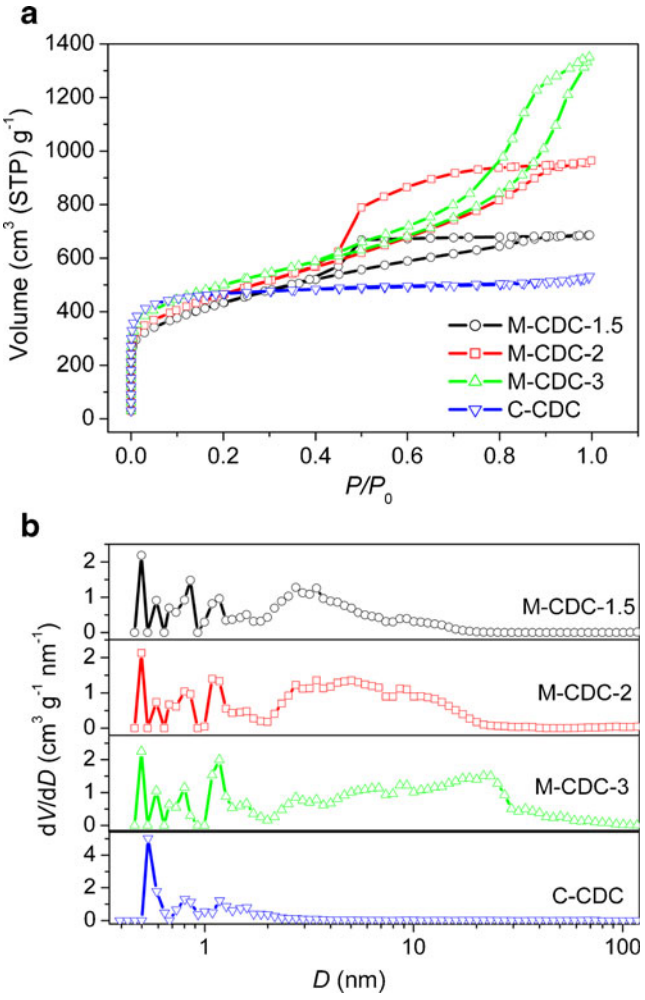

Fig. 3 N_2 adsorption–desorption isotherms (**a**) and resultant DFT pore size distributions (**b**) of C-CDC and M-CDC samples

of ions into inner surface of electrode materials. The fast ions transport is beneficial to capacitance retention. Pore structures of M-CDC samples are superior to those of C-CDC, which are convenient for ions transports in porous electrode.

Figure 6a, b compares CV properties of M-CDC with those of C-CDC at 20 and 100 Mv s^{-1}. The area of CV curves can reflect the capacitance values, which is accordant with the results from galvanostatic charge/discharge. The rectangular degree can be used to assess the ion diffusion rate within nanoporous carbon structure. The higher the rectangle degree, the faster the kinetic process rate. At low voltage sweep rate of 20 mV s^{-1}, the electrolyte ions have sufficient time to penetrate into the inner pore; thus, all samples exhibit rectangular-shaped CV curves. With the scan rate increasing up to 100 mV s^{-1}, M-CDC materials give the excellent capacitive behaviors as observed from rectangular degree of their CV curves. The voltammogram of C-CDC becomes slightly distorted indicative of an unacceptable capacitive performance. The superior kinetic process of M-

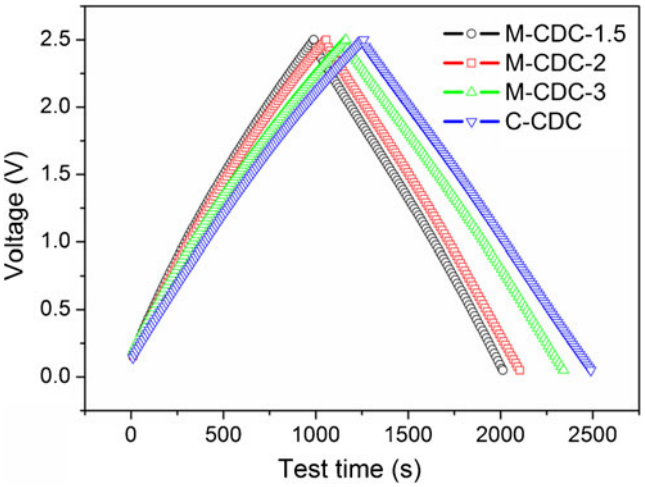

Fig. 4 Galvanostatic charge/discharge curves for C-CDC and M-CDC samples

CDC is believed to be associated with its advantageous microstructure over C-CDC. For C-CDC, its restricted texture, pure, and interior micropores lead to high resistance for ion transport and long distance (about 4 μm, half of the particle size) for electrolyte diffusion. Large values of these two parameters would cause significant electrochemical impedance and a low ion-accessible surface area at a high voltage sweep rate, thus severely reducing the rate performance of EC. On the contrary, the 3-D network of M-CDC would be easily wetted with electrolyte as compared to micropores of conventional CDC. And ion-buffering reservoirs can be formed in the gel architecture to minimize the diffusion distance to the interior surface area. Meanwhile, the short pores channel linked to the small particle size (20–100 nm) of TiC unit would become critical for the improvement in ion migration. On the other hand, mostly

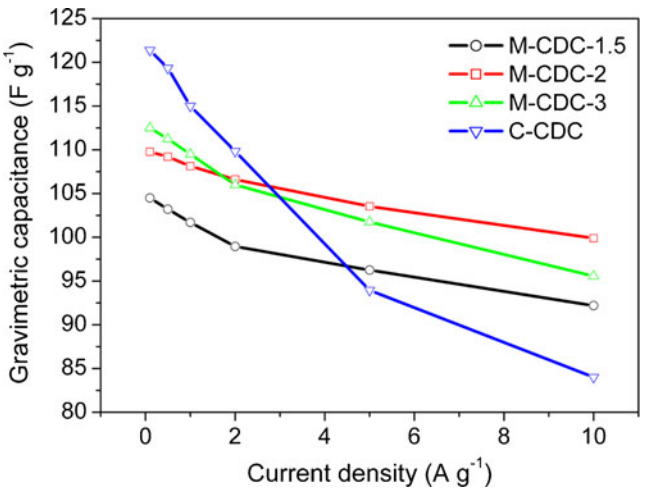

Fig. 5 Comparison of capacitance retention with increasing current density for C-CDC and M-CDC samples

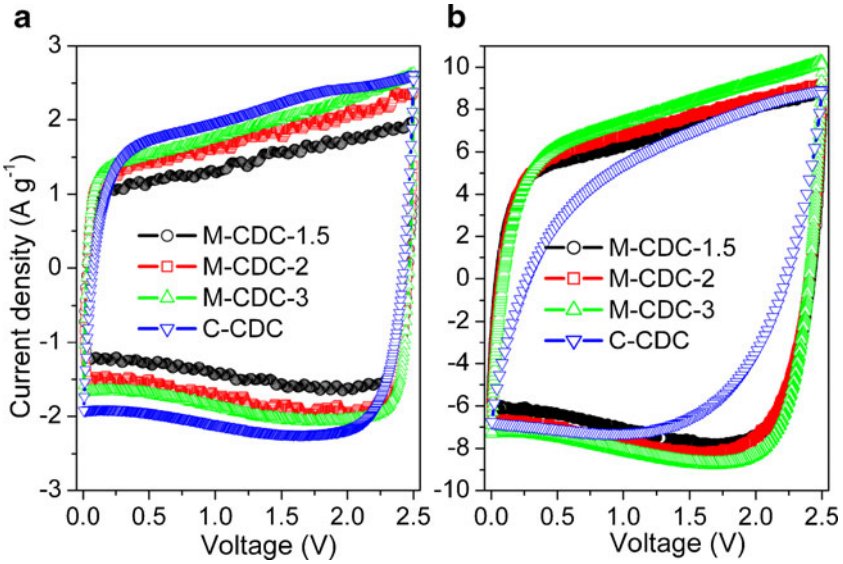

Fig. 6 Cyclic voltammograms for C-CDC and M-CDC samples at the voltage sweep rate of 20 mV s^{-1} (**a**) and 100 mV s^{-1} (**b**)

exterior surface areas would also contribute to achieving distinguished capacitive behaviors.

Although the CV can be utilized to evaluate the ion transport behaviors, it is still unable to precisely describe the actual electrochemical diffusion process. Hence, it is quite important to further investigate the influence of pore architecture on ion diffusion based on EIS, which is considered to be a powerful method for obtaining the dynamic information of ion diffusion [30, 31]. Figure 7 demonstrates the dependence of capacitance (C) on the frequency, according to the equation $C = Z''/(2\pi f|Z|^2)$, where Z'' is the imaginary part of impedance [22]. This type of plot provides a convenient method to show the frequency response of EC because frequency is the dependant variable, unlike Nyquist plots that have frequency buried in both the real and imaginary impedance terms. Capacitance–frequency dependence can investigate the penetration of the alternating current into the bulk pores of the electrode materials and illustrate how many surface areas can be accessible to solvated ions at a specific frequency. The relative performances of all carbons confirm the results from charge–discharge tests. All the curves present a transition between purely resistive behaviors, where C is equal to zero to purely capacitive behavior where C reaches its maximum value. The capacitance of C-CDC does not exhibit signs of saturation at 0.01 Hz, suggesting the larger particle size and longer diffusion distance for electrolyte ions prevent the system from reaching the ion adsorption equilibrium within ~100 s period. In contrast, most of the electrolyte ions reach the adsorption sites in the bulk of M-CDC. We define the limiting frequency at which the capacitance decreases by no more than 50%. In comparison to that of C-CDC, the limiting frequency for M-CDC-2 exceeds 1.17 Hz, while for strictly C-CDC, the limiting

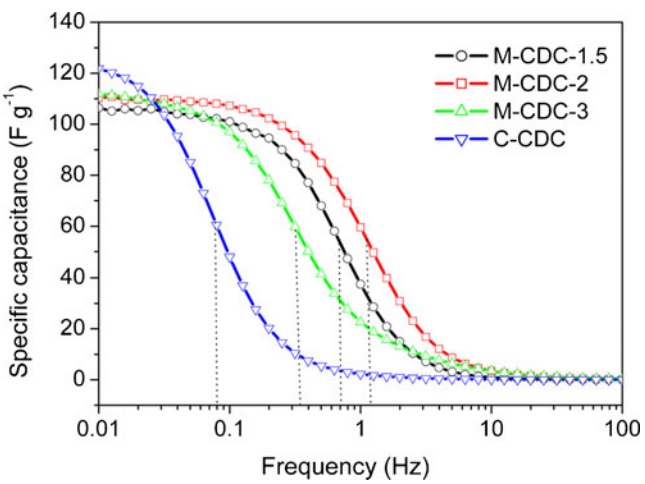

Fig. 7 Capacitance variation with frequency for all CDC samples

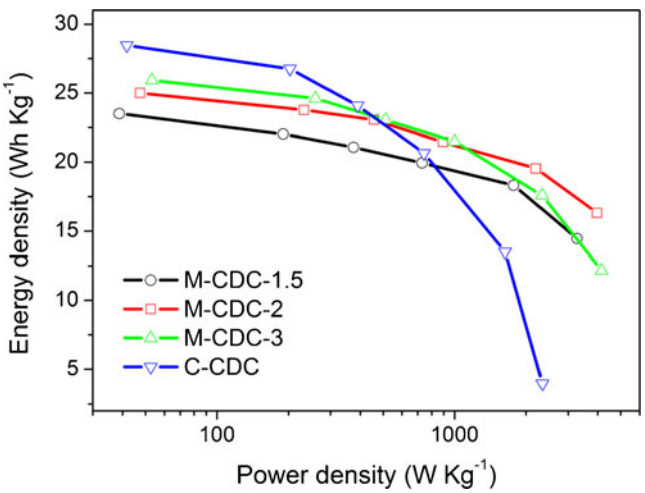

Fig. 8 Ragone-type plots of energy density versus power density

frequency is less than 0.08 Hz. The restricted sluggish diffusion of electrolyte ions into inner pores can be explained. It is worthy to note that M-CDC-2 demonstrates the best frequency response as compared to M-CDC-1.5 and M-CDC-3 with the limiting frequency of 0.67 and 0.32 Hz, respectively. These results might be associated with the difference in the amount of residual free carbons, which are considered to play an important role on the electrode kinetic process. For the EC, the complete wetting with electrolyte is most desired. Reasonable amount of free carbons maybe make M-CDC material more solvophilic and enhance the wetting properties of individual pores, which need to be confirmed through the further study. However, excess free carbons in M-CDC-1.5 would block the transfer/diffusion of ions in the M-CDC matrix to a certain extent, leading to the poor frequency response. On the other hand, results aforementioned could also be attributed to the difference in proportion of mesopores. Among all samples, M-CDC-2 owns the largest amount of mesopores surface areas, which deliver the best capacitance retention and frequency response.

The Ragone plots for the CDC carbons are shown in Fig. 8, which reveals the dependence between power output and energy density. The energy (E) is calculated as $E = (1/2)CV^2$, where C is the capacitance of the two-electrode cell calculated from galvanostatic tests (1/4 single electrode capacitance) and V is the voltage decrease in discharge. The power (P) is calculated as $P = E/\Delta t_d$, where E is the energy and Δt_d is the time spent in discharge. The energy density and power density are calculated by dividing W and P by the total mass of carbons in the EC. As observed from the Ragone plots, M-CDC materials show quite superior properties to C-CDC. For C-CDC, as the power density increases from 40 to 2,300 W kg^{-1}, energy density drops dramatically from 28.5 to 3.8 Wh kg^{-1}. Comparatively, M-CDC samples still maintain high energy density (11.9–16.3 Wh kg^{-1}) even at much higher power density (4,280 W kg^{-1}). The energy and power limitations normally observed at high rates are associated with the electrode kinetic process within the porous textures. The outstanding energy properties of M-CDC clearly confirm the success of optimized pore architecture for faster ions migration into the bulk of the CDC particles and higher utilization efficiency of surface areas.

Conclusions

In this paper, a successful strategy to optimize the pore texture of CDC for their application in electrochemical capacitors is realized by using as-synthesized mesoporous TiC as precursors. It is possible to vary the pore architecture of CDC to a greatly extent and overcome the poor control over pore-size distribution, which is purely adjusting by changing starting materials and chlorine etching temperature for conventional CDC materials. The 3-D network of as-prepared M-CDC is beneficial for the electrolyte wetting and electron conduction along the carbon skeleton. Moreover, the significantly reduced dimension of particle unit decreases the electrolyte diffusion route with the nanometer-scaled level. As a result, M-CDC possess superior capacitance retention of 90% at 10 A g^{-1} and frequency response as compared to the C-CDC produced from dense nonporous TiC.

Acknowledgments This work was partly supported by National Science Foundation of China (No. 50730003), and Technology Talent Foundation of Shanghai.

References

1. Conway BE (1999) Electrochemical supercapacitors. Kluwer Academic/Plenum, New York
2. Winter M, Brodd RJ (2004) Chem Rev 104:4245–4269
3. Service RF (2006) Science 313:902
4. Miller JR, Simon P (2008) Science 321:651–652
5. Simon P, Gogotsi Y (2008) Nat Mater 7:845–854
6. Arico AS, Bruce P, Scrosati B, Tarascon JM, Schalkwijk WV (2005) Nat Mater 4:366–377
7. Huang JS, Sumpter BG, Meunier V (2008) Angew Chem Int Ed 47:520–524
8. Huang J, Sumpter BG, Meunier V (2008) Chem Eur J 14:6614–6626
9. Chmiola J, Largeot C, Taberna PL, Simon P, Gogotsi Y (2008) Angew Chem Int Ed 47:3392–3395
10. Salitra G, Soffer A, Eliad L, Cohen Y, Aurbach D (2000) J Electrochem Soc 147:2486–2493
11. Wang DW, Li F, Liu M, Lu GQ, Cheng HM (2008) Angew Chem Int Ed 47:373–376
12. Lin R, Taberna PL, Chmiola J, Guay D, Gogotsi Y, Simon P (2009) J Electrochem Soc 156:A7–A12
13. Largeot C, Portet C, Chmiola J, Taberna PL, Gogotsi Y, Simon P (2008) J Am Chem Soc 130:2730–2731
14. Eikerling M, Kornyshev AA, Lust E (2005) J Electrochem Soc 152:E24–E33
15. Mysyk R, Raymundo-Pinero E, Pernak J, Beguin F (2009) J Phys Chem C 113:13443–13449
16. Mysyk R, Raymundo-Pinero E, Beguin F (2009) Electrochem Commun 11:554–556
17. Pandolfo AG, Hollenkamp AF (2006) J Power Sources 157:11–27
18. Gogotsi Y, Nikitin A, Ye H, Zhou W, Fischer JE, Yi B, Foley HC, Barsoum MW (2003) Nat Mater 2:591–594
19. Shanina BD, Konchits AA, Kolesnik SP, Veynger AI, Danishevskii AM, Popov VV, Gordeev SK, Grechinskaya AV (2003) Carbon 41:3027–3036
20. Arulepp M, Leis J, Latt M, Miller F, Rumma K, Lust E, Burke AF (2006) J Power Sources 162:1460–1466
21. Janes A, Lust E (2006) J Electrochem Soc 153:A113–A116
22. Chmiola J, Dash R, Yushin G, Gogotsi Y (2006) J Power Sources 158:765–772
23. Chmiola J, Yushin G, Gogotsi Y, Portet C, Simon P, Taberna PL (2006) Science 313:1760–1763
24. Chmiola J, Yushin G, Dash RK, Hoffman EN, Fischer JE, Barsoum MW, Gogotsi Y (2005) Electrochem Solid State Commun 8:A357–A360
25. Portet C, Yushin G, Gogotsi Y (2008) J Electrochem Soc 155: A531–A536

26. Korenblit Y, Rose M, Kockrick E, Borchardt L, Kvit A, Kaskel S, Yushin G (2010) ACS Nano 4:1337–1344
27. Chmiola J, Largeot C, Taberna PL, Simon P, Gogotsi Y (2010) Science 328:480–483
28. Cheng G, Long DH, Liu XJ, Ling LC (2009) New Carbon Mater 24:243–250
29. Dash RK, Yushin G, Gogotsi Y (2005) Micropor Mesopor Mater 86:50–57
30. Sugimoto W, Iwata H, Yokoshima K, Murakami Y, Takasu YJ (2005) J Phys Chem B109:7330–7338
31. Song HK, Hwang HY, Lee KH, Dao LH (2000) Electrochim Acta 45:2241–2257